ChemElectroChem

Research Article
doi.org/10.1002/celc.202500162

Chemistry Europe
European Chemical Societies Publishing

www.chemelectrochem.org

Enhancing Sodium-Ion Battery Performance: The Role of Glyoxylic Acetal-Based Electrolytes in Solid Electrolyte Interphase Formation and Stability

Mariana Gaško, Christian Leibing, Lukas Fridolin Pfeiffer, Peter Axmann, Andrea Balducci,* and Maider Zarrabeitia*

This study systematically investigates the feasibility of replacing conventional sodium hexafluorophosphate ($NaPF_6$) in carbonate-based electrolytes with sodium bis(fluorosulfonyl)imide (NaFSI) and sodium bis(trifluoromethanesulfonyl)imide (NaTFSI) in a 1,1,2,2-tetraethoxyglyoxal (TEG):propylene carbonate (PC) solvent system tested with hard carbon (HC) anode materials for sodium-ion batteries (SIBs). The influence of electrolyte composition and cycling conditions on the evolution of the solid electrolyte interphase (SEI) and overall electrochemical performance of the HC is comprehensively evaluated by means of electrochemical impedance spectroscopy and X-ray photoelectron spectroscopy. The SEI chemical composition, transport properties, and stability are thoroughly characterized. The results demonstrate that the HC tested in NaFSI/TEG:PC electrolyte exhibits superior performance compared to both the conventional $NaPF_6$/ethylene carbonate (EC):PC system and the NaTFSI/TEG:PC-based alternative, achieving higher initial coulombic efficiencies (ICEs), lower interfacial resistance, and enhanced Na^+ transport properties. The improved electrochemical stability of the HC in NaFSI/TEG:PC electrolyte is attributed to the formation of a bilayered SEI, comprising an inorganic-rich inner layer and an organic-rich outer layer. These findings underscore the pivotal role of electrolyte formulation in enhancing the HC SEI characteristics and cycling performance, thereby positioning NaFSI in TEG:PC chemistry as a promising electrolyte candidate for next-generation SIBs.

1. Introduction

The rapid expansion of renewable energy sources, the increasing electrification of transportation, and the rising use of portable electronics have unequivocally heightened the demand for efficient, sustainable, and cost-effective energy storage solutions.[1] To date, lithium-ion technology has dominated the global market due to its high energy density, superior long-term cycling performance, and lower self-discharge compared to other battery systems.[2] However, concerns over the availability and geopolitical implications of lithium (Li) and cobalt (Co) resources have prompted researchers to seek promising, sustainable, and cost-effective alternatives. Post-lithium battery systems, such as sodium-ion and potassium-ion batteries (PIBs), are attracting increasing attention due to their advantages over Li technology. Sodium (Na) and potassium (K) are more widely distributed and readily available within the Earth's crust and the ocean.[3,4] Moreover, unlike Li, which forms alloys with aluminum (Al), using lightweight and cheaper Al current collectors, as opposed to copper (Cu), is feasible. These benefits collectively facilitate reductions in both total cell mass and materials cost while simultaneously enhancing the overall energy density of the cell.[5] Although PIBs are currently in the early stages of development, the Group 1 company has already released the 1st PIB prototype.[6] Regarding sodium-ion batteries (SIBs), Natron Energy has initiated their production at a commercial scale in the United States, while Faradion, Tiamat, HiNa Batteries, and CATL are the leading companies commercializing SIBs in the EU and China, respectively.[7–9] Researchers anticipate that Na-based technology might exhibit superior performance relative to Li systems in terms of electrochemical stability and operational safety, demonstrating greater potential for long-term reliability, as well as being sustainable and cost-effective. Currently, SIBs commonly utilize hard carbon (HC) as anode material and non-aqueous electrolytes that contain sodium hexafluorophosphate ($NaPF_6$) as the conducting salt in a blend of carbonate-based solvents, such

M. Gaško, M. Zarrabeitia
Helmholtz Institute Ulm (HIU)
Helmholtzstrasse 11, 89081 Ulm, Germany
E-mail: maider.ipina@kit.edu

M. Gaško, M. Zarrabeitia
Karlsruhe Institute of Technology (KIT)
76021 Karlsruhe, Germany

M. Gaško, C. Leibing, A. Balducci
Institute for Technical Chemistry and Environmental Chemistry
Friedrich Schiller University Jena
Philosophenweg 7a, 07743 Jena, Germany
E-mail: andrea.balducci@uni-jena.de

C. Leibing, A. Balducci
Center for Energy and Environmental Chemistry Jena (CEEC Jena)
Friedrich Schiller University Jena
Philosophenweg 7a, 07743 Jena, Germany

L. Fridolin Pfeiffer, P. Axmann
ZSW Center for Solar Energy and Hydrogen Research Baden-Württemberg
Helmholtzstrasse 8, 89081 Ulm, Germany

Supporting information for this article is available on the WWW under https://doi.org/10.1002/celc.202500162

as ethylene carbonate (EC), diethyl carbonate, dimethyl carbonate (DMC), or propylene carbonate (PC).[10–12] These solvents are typically combined in a specific ratio to take advantage of their high dielectric constants and low viscosity, which aids the movement of Na^+ and provides broad electrochemical stability.[10]

Despite their benefits, recent studies suggest that the decomposition byproducts of carbonate-based Na electrolytes exhibit increased solubility, potentially leading to continuous parasitic reactions and thickening of the solid electrolyte interphase (SEI).[13] This phenomenon limits the transport properties and negatively impacts the long-term performance of SIBs, hindering the widespread application. Current research focuses on substituting carbonate-based solvents with ether-based ones to create a stable and compact SEI.[14] Their utilization has resulted in enhanced chemical compatibility with the active materials, ultimately leading to a favorable SEI with superior Na^+ migration properties.[15–17]

In this context, the potential of using 1,1,2,2-tetraethoxyglyoxal (TEG) as an electrolyte component appears promising. TEG is a commercially available glyoxal-based solvent that offers several advantages, including higher boiling and flash points compared to linear carbonate-based solvents, as well as lower viscosity in comparison to cyclic carbonates.[18,19] These characteristics enhance operational safety and facilitate Na^+ diffusion. The effectiveness of glyoxal-based solvents in various energy storage devices, such as electrochemical double-layer capacitors, lithium-ion batteries (LIBs), and PIBs, has already been successfully demonstrated.[19–21] Furthermore, TEG has shown improved interface-forming properties on carbon-based electrodes for LIBs, underscoring its potential.[22] Recently, its use in SIBs has also been reported.[23] However, a comprehensive analysis of the chemical composition of the SEI on HC for SIBs, its stability during cycling, and a fundamental understanding of how electrochemical cycling conditions influence SEI formation have yet to be conducted. Given the challenges in predicting SEI formation, an in-depth study of the various parameters that affect SEI is essential.

Hence, this study aims to investigate the composition and chemical stability of the SEI and its impact on the electrochemical performance of commercial HC anode material for SIBs. For this purpose, half-cells containing HC as the active material and various electrolytes were utilized. The electrolytes under investigation include 1M $NaPF_6$ in EC:PC (1:1 vol.%), which is considered the standard electrolyte for this study. The potential for partially replacing carbonate-based solvents with alternative electrolyte systems, such as 1M sodium bis(trifluoromethanesulfonyl)imide (NaTFSI) and 1M sodium bis(fluorosulfonyl)imide (NaFSI), both in a mixture of TEG and PC (3:7 wt.%), is examined in detail.

2. Results and Discussion

In this study, Na-based half-cells containing commercial HC as the working electrode and three different electrolyte formulations, including 1M $NaPF_6$ in EC:PC (1:1 vol.%), 1M NaTFSI in TEG:PC (3:7 wt.%), and 1M NaFSI in TEG:PC (3:7 wt.%), were studied. The mass ratio of TEG to PC was established at 3:7 wt.% based on prior research conducted by our group.[24] This formulation has demonstrated optimal physicochemical properties, particularly in terms of ionic conductivity and viscosity, as reported in the literature. Moreover, incorporating PC into the NaTFSI in TEG:PC electrolyte has been previously investigated, showing an increase in the positive potential limit to 4.3 V versus Na^+/Na, whereas the pure TEG electrolyte exhibited an upper cutoff voltage of only 3.9 V versus Na^+/Na.[23] A similar trend is observed with NaFSI in the TEG:PC electrolyte, which demonstrates anodic stability up to 4.5 V versus Na^+/Na (see Figure S1, Supporting Information). Meanwhile, the cathodic stability is unaffected by the addition of TEG or the replacement of $NaFP_6$ salt with NaTFSI or NaFSI. This finding highlights the potential for enhancing the electrochemical stability window of these systems, making them suitable for full cells, such as using sodium transition metal oxides as a cathode that requires an upper cutoff potential exceeding 4 V versus Na^+/Na.

The primary parameters altered in this study were the C-rate applied during the SEI formation and the electrolyte chemistry. The current rate applied during the 1st cycle is critical, as it directly influences the electrolyte decomposition and thereby governs the formation of the SEI, ultimately affecting the overall electrochemical performance of the battery. Excessively high currents can lead to incomplete SEI formation, resulting in instability and diminished performance over cycles.[25] Conversely, choosing a too low initial C-rate prolongs the time required for forming the SEI, resulting in higher electrical energy consumption. This is particularly significant in large-scale battery production, where reducing the time required for SEI formation can lower energy consumption, and consequently, decrease overall production costs.[26] The herein-chosen current densities for the SEI formation cycle are 4 and 10 mA g^{-1}, which equals C/50 and C/20 (considering 1C = 200 mAh g^{-1}). The electrolytes used in this work comprise a conventional formulation acting as a comparative standard (1 M $NaPF_6$ in EC:PC (1:1 vol.%)) and two novel electrolytes that provide improved safety characteristics (1 M NaTFSI and 1 M NaFSI, both in a mixture of TEG and PC (3:7 wt.%)).[23,27]

2.1. Electrochemical Performance of HC Anodes with Different Electrolytes

Figure 1a,b depicts the 1st charge/discharge cycle at current densities of C/50 and C/20 for HC systems based on 1M NaFSI in TEG:PC and NaTFSI in TEG:PC electrolytes. The typical potential profile of HC is visible for both systems, exhibiting the characteristic high-voltage sloping region (>0.1 V vs Na^+/Na) and low-voltage plateau (<0.1 V vs Na^+/Na). These regions correspond to the well-documented Na^+ storage mechanisms in HC, which include the adsorption of Na^+ at defect and edge sites, and the insertion of Na^+ into micropores.[28,29] The HC systems utilizing NaFSI/TEG:PC, and NaTFSI/TEG:PC demonstrate similar Na^+ storage behavior to the standard $NaPF_6$-based electrolyte (Figure S2, Supporting Information), with slope/plateau capacities yielding approximate values of 144/185, and 146/180 mAh g^{-1} at C/50, and 131/164, and 134/171 mAh g^{-1} at C/20, for the HC tested in NaFSI/TEG:PC, and NaTFSI/TEG:PC electrolytes, respectively

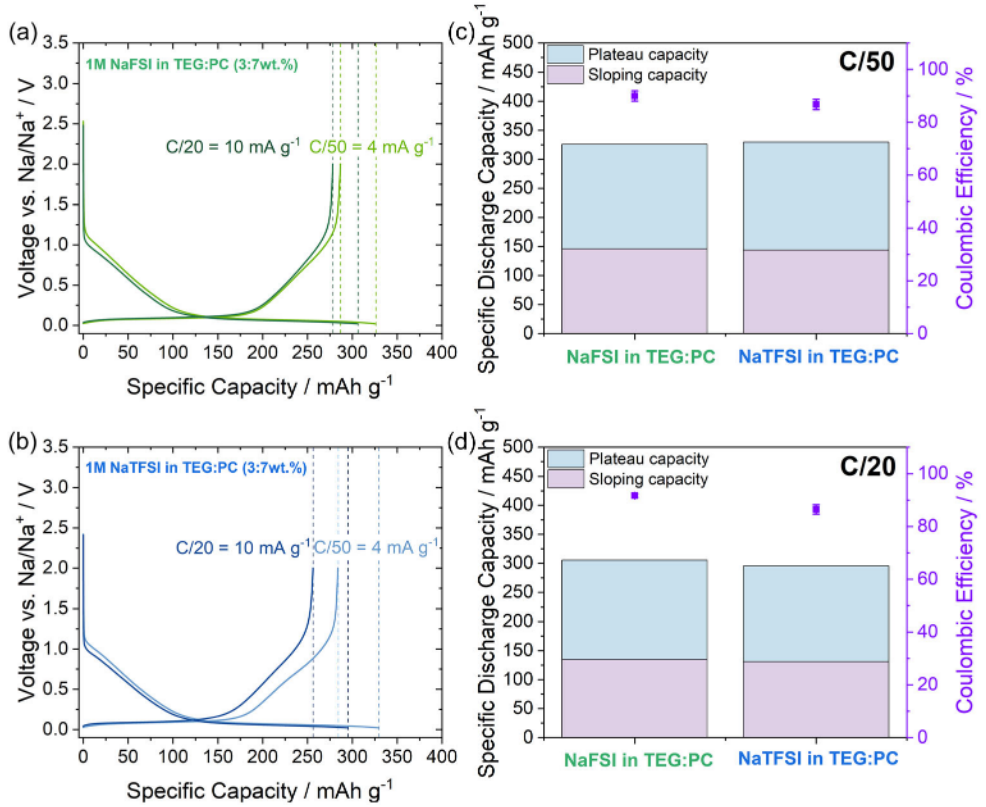

Figure 1. 1st potential profiles of HC tested in a) 1 M NaFSI in TEG:PC, and b) 1 M NaTFSI in TEG:PC electrolytes at two different C-rates, e.g., C/50 (light color) and C/20 (dark color). Contribution of slope and plateau capacity of the 1st discharge and ICE of HC electrodes using both electrolytes at rates of c) C/50 and d) C/20.

(Figure 1c,d). Increased capacity is anticipated to be observed at lower C-rates, as a reduced C-rate prolongs the duration of both discharge and charge cycles. This extended time frame facilitates greater penetration of Na^+ into the microstructure of HC, subsequently enhancing its storage capabilities. The comparable performance of the HC in NaFSI/TEG:PC and NaTFSI/TEG:PC electrolytes, compared to the well-documented $NaPF_6$/EC:PC, suggests good compatibility between the HC and the novel electrolytes developed, regardless of the initial C-rate. This compatibility is further evidenced by the high initial coulombic efficiency (ICE) of HC, which remains consistent across the different electrolytes used.

The ICE of HC when the formation cycle was conducted at C/50 decreases in the following order: NaFSI/TEG:PC > $NaPF_6$/EC:PC > NaTFSI/TEG:PC, yielding values of (90 ± 2)%, (88 ± 2)%, and (87 ± 2)%, respectively. The same trend is observed for the C/20 formation cycle of HC, with the obtained ICEs being (92 ± 1)%, (89 ± 1)%, and (86 ± 2)% when tested in NaFSI/TEG:PC, $NaPF_6$/EC:PC, and NaTFSI/TEG:PC, respectively. It can be inferred that increasing the C-rate from C/50 to C/20 would enhance the ICE of HC by reducing the kinetics of electrolyte decomposition. This would mitigate the loss of Na^+ resulting from electrolyte consumption. However, the herein-presented findings reveal no significant differences between the C-rate applied during the formation cycle for HC systems employing $NaPF_6$/EC:PC, NaFSI/TEG:PC, and NaTFSI/TEG:PC electrolytes. This suggests that the discrepancies in ICE are primarily influenced by the microstructure of HC itself rather than by the electrolyte used or the applied C-rate. This can be attributed to the inherently disordered structure of HC, which affects pore accessibility, and consequently, influences the achievable charge and discharge capacities. Thus, modifying the precursor used in the synthesis of HC or the pre-treatment steps primarily impacts its microstructure, thereby affecting its interaction with the electrolyte and overall electrochemical performance (such as delivered specific capacity, cycling stability, and rate performance). This has been previously observed by our group using different bio-waste precursors or modifying the synthetic parameters, but with the same precursor.[30–32]

The rate performance of HC electrodes in the chosen electrolytes was further evaluated by first conducting an initial formation cycle at current densities of either C/50 or C/20. This was followed by five cycles at progressively increasing rates: C/10, C/5, C/3, C/2, and 1C. Then, returning to C/5 and concluding with a test at C/2 to assess cycling performance (**Figure 2**). The measurements were performed three times, and the standard deviation was calculated following Equation (S1) provided in the Supporting Information.

Firstly, it is noted that the CEs of the HC, regardless of the initial C-rate and electrolyte chemistry, range from 99.75 to 99.99%. This suggests strong reversibility of the Na^+ (de) insertion mechanism in HC for both electrolytes. Among the evaluated systems, the incorporation of NaFSI in TEG:PC enhances the HC rate performance compared to the NaTFSI-based system, regardless of the C-rate applied during the formation cycle. Specifically,

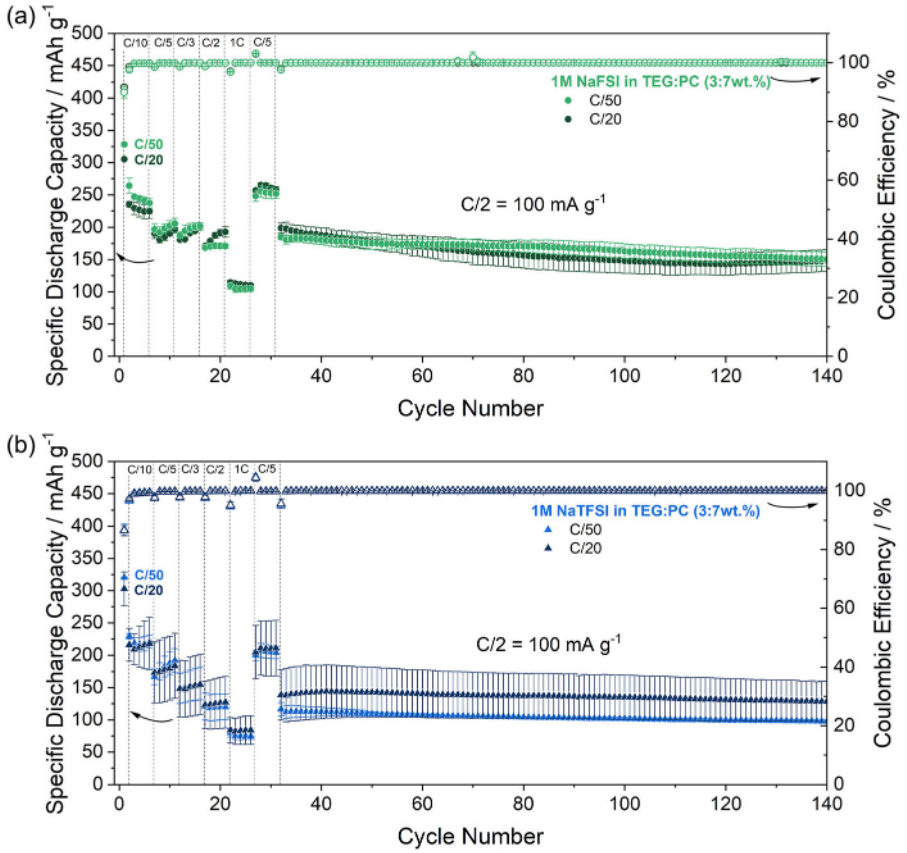

Figure 2. Rate capability and cycling performance of HC tested in a) 1 M NaFSI in TEG:PC, and b) 1 M NaTFSI in TEG:PC electrolytes after the 1st cycle at C/50 (light color) and C/20 (dark color). The bars indicate the standard deviation.

at a C-rate of 1C, the capacity retention relative to the 1st cycle is 37 and 28% for C/20 and 33% and 25% for C/50, in the NaFSI- and NaTFSI-based systems, respectively. These findings indicate that increasing the C-rate from C/50 to C/20 improves the HC rate performance for both electrolytes. A similar trend is observed for the standard $NaPF_6$-based electrolyte, which exhibits capacity retentions of 38% at C/20 and 31% at C/50 when the C-rate is increased to 1C (see Figure S3, Supporting Information). Interestingly, a distinct trend is observed in the cycling performance of HC. Specifically, at a C-rate of C/2, the capacity retention (after 140 cycles, relative to the 32nd cycle) is 93 and 75% for the C/20 condition, and 84 and 81% for the C/50 condition in the NaTFSI/TEG:PC- and NaFSI/TEG:PC-based systems, respectively. These findings initially suggest that using a current density of C/20 during the 1st cycle in HC systems containing the NaTFSI-based electrolyte enhances both cycling stability and rate performance. However, when factoring in the standard deviation and associated error margins, the difference in performance between the C/50 and C/20 formation conditions becomes negligible. This indicates comparable electrochemical performance between the two conditions, with the key distinction being that HC systems utilizing NaTFSI/TEG:PC electrolyte exhibit higher statistical reliability when subjected to C/50 during the 1st cycle. In contrast, HC tested with NaFSI in TEG:PC exhibits a 6% higher capacity retention, demonstrating superior cycling performance when initially subjected to C/50 compared to C/20. A similar trend is observed for the $NaPF_6$-based system, which undergoes more pronounced capacity degradation when initially cycled at C/20, suggesting comparable electrochemical performance between these two electrolytes. The corresponding dQ/dV plots (Figure S4, Supporting Information) indicate that the superior cycling performance observed when initially subjected to C/50 is likely related to a lower overpotential in the $NaPF_6$- and NaFSI-based systems. Overall, the comparative analysis of the tested electrolytes indicates that NaFSI in TEG:PC presents a greater potential than NaTFSI in TEG:PC as a viable alternative to the conventional $NaPF_6$-based electrolyte, particularly when subjected to C/50 during the formation cycle (see Figure S5, Supporting Information). In comparison, the notably lower capacity observed of HC using NaTFSI in TEG:PC can be linked to a significantly increased voltage hysteresis, as illustrated in Figure S4c, Supporting Information. This pronounced hysteresis indicates a higher level of polarization and suggests a kinetic limitation in Na^+ transport.

Given that commercial HC is employed as the electrode material, the electronic and ionic conductivity of the active material should remain consistent across all systems, excluding these factors as potential sources of the observed electrochemical differences. Furthermore, the comparable transport properties of the investigated TEG-based electrolytes and the absence of significant variations in the 1st cycle performance suggest that discrepancies emerging during continuous cycling are primarily associated with the SEI. In particular, the SEI's chemical

composition and long-term stability appear to be critical determinants, as they directly influence Na^+ migration. Consequently, these properties likely govern the differences in electrochemical performance observed among the tested electrolyte systems. This claim is supported by comparing the corresponding potential profiles from the previously discussed rate and cycling performance (Figure S6, Supporting Information). The gradual decline in capacity observed between cycles 30 and 140 is primarily attributed to a decrease in the low-voltage plateau capacity, suggesting a reduced (de-)insertion of Na^+ into the microstructure of HC. This indicates a progressive loss in the ability of HC to store Na^+ reversibly. The accessibility of the porous structure of HC is strongly dependent on the characteristics of the established SEI and the associated Na^+ transport properties, which will be discussed in detail in the following sections.

2.2. Transport Properties and Chemical Composition of the SEI Formed on the HC Anodes with Different Electrolytes

To evaluate the stability of the formed SEI and the resulting Na^+ transport properties of the HC electrodes, electrochemical impedance spectroscopy (EIS) was conducted after the 1st cycle at both C-rates (i.e., C/50 and C/20), and subsequently after the 6th, 11th, 16th, 21st, and 26th cycles at C/2 (in the discharged state = sodiated HC). The results have been visualized in Nyquist plots, presented in **Figure 3**a–d. The presented Nyquist curves can be classified into two distinct regions, corresponding to the charge-transfer resistance (R_{ct}) of Na^+ in the medium-frequency region and the interfacial resistance (R_{SEI}) associated with SEI formation in the high-frequency region, indicating similar electrochemical processes among the investigated electrolytes.[14] Notably, R_{ct} is more pronounced than R_{SEI} for all systems, indicating that the migration resistance of Na^+ across the HC surface significantly contributes to the overall impedance. This highlights the importance of establishing a stable SEI, which helps to reduce continuous electrolyte consumption, and thus, enhances the unhindered diffusion of Na^+ across the SEI into the HC bulk structure. EIS measurements indicate that the choice of electrolyte formulation has a significant impact on the system's overall resistance. For HC utilizing NaFSI- and NaTFSI-based electrolytes, a consistent decline in overall resistance is observed after the 1st cycle, irrespective of the initial C-rate. In contrast, for the HC tested in a $NaPF_6$-based system, the initial C-rate has a significant impact on the resistance evolution. In fact, the overall resistance in a $NaPF_6$-based system decreases progressively over cycling when a C-rate of C/20 is applied during the 1st cycle. However, with a formation cycle of C/50, the system experiences a continuous increase in resistance, suggesting the development of a less stable SEI (Figure S7a,b, Supporting Information).

To further quantify the extent of the SEI's evolution over cycling and its effect on Na^+ transport kinetics, the contribution of R_{SEI} and R_{ct} was further quantified by fitting the EIS curves with the equivalent circuit presented in Figure 3f. R_s denotes the ohmic resistance of the entire three-electrode Swagelok setup, R_{SEI} represents the interfacial resistance for Na^+ migration across the SEI, and R_{ct} represents the charge-transfer resistance in HC, while *CPE*1 and *CPE*2 are constant-phase elements of each process.[33] The evolution of R_{SEI} and R_{ct} is presented in Figure 3e–h. A summary of the fitted parameter values is provided in Table S1–S6, Supporting Information. HC paired with NaFSI in TEG:PC shows noticeable differences between the two SEI formation conditions, in terms of resistance values. R_{SEI} and R_{ct} continuously decrease from 29 to 14 Ω and from 231 to 85 Ω, respectively, over cycles for the initial cycle at C/50. In the case of the R_{SEI} and R_{ct}, when the initial cycle was at C/20, a decrease is observed, although to a lesser extent, with values maintaining ≈5 and 50 Ω, respectively. Conversely, the differences between the two formation conditions are not particularly pronounced for the NaTFSI-based system, as R_{SEI} stabilizes after 6 to 11 cycles, exhibiting values of 7 Ω for C/50 and 6 Ω for C/20. A similar trend is evident for R_{ct}, which shows minimal changes for C/50 (R_{ct}: 100–80 Ω) and C/20 (R_{ct}: 90–80 Ω) after stabilization following the 11th cycle.

Consistent with this observation, HC, utilizing the standard $NaPF_6$ in EC:PC electrolyte, forms a stable SEI with reduced resistance to Na^+ migration during the C/20 formation cycle. This stability is evidenced by the stabilization of R_{SEI} between the 5th and 26th cycles, with a consistent value of 5–6 Ω. Furthermore, the decrease in R_{ct} from 174 to 130 Ω after the 5th cycle indicates a net improvement in Na^+ transport properties over prolonged cycling. In contrast, HC cells initially cycled at C/50 exhibit a significant increase in both R_{SEI} and R_{ct} after the 5th cycle, rising from 3 to 46 Ω and from 270 to 546 Ω, respectively, suggesting instability of the SEI formed under these conditions (Figure S7c,d, Supporting Information). EIS results indicate that subjecting the HC electrodes to an initial formation cycle at C/20 results in the formation of a probably thinner SEI, with reduced resistance to Na^+ (de)insertion kinetics within the HC structure among all investigated electrolytes (note that for the NaTFSI-based system, no pronounced differences between both formation cycles were observed). This observation aligns with the findings from the electrochemical analysis. Notably, the cycling performance of HC in NaFSI/TEG:PC (see Figure 2a) slightly improves when a current density of C/50 is applied during the 1st cycle (6% more capacity retention than when initially tested at C/20). Although the increased R_{SEI} and R_{ct} initially might suggest the formation of a more resistive SEI, potentially due to its composition or thickness (the latter hypothesis confirmed by X-ray photoelectron spectroscopy (XPS), see XPS section for further explanation of R_{SEI} trend). Nevertheless, this does not result in the expected deterioration of electrochemical performance. Instead, both R_{SEI} and R_{ct} decrease with increasing cycle numbers, indicating that the passivation properties of the SEI improve despite its evolution, thereby facilitating Na^+ diffusion during continuous cycling.

The stability and chemical composition of the SEI were further analyzed using XPS on cycled HC electrodes. This analysis was conducted after the 1st cycle at C/50 and C/20, as well as after 15 cycles at C/2 (at the discharged state). The electrodes were cleaned with DMC and dried prior to measurement. The high-resolution C 1*s* (**Figure 4**) and F 1*s* spectra (**Figure 5**), which illustrate the decomposition products of the solvent and the byproducts resulting from the salt decomposition, are explored in greater detail. Additionally, the high-resolution S 2*p* spectra

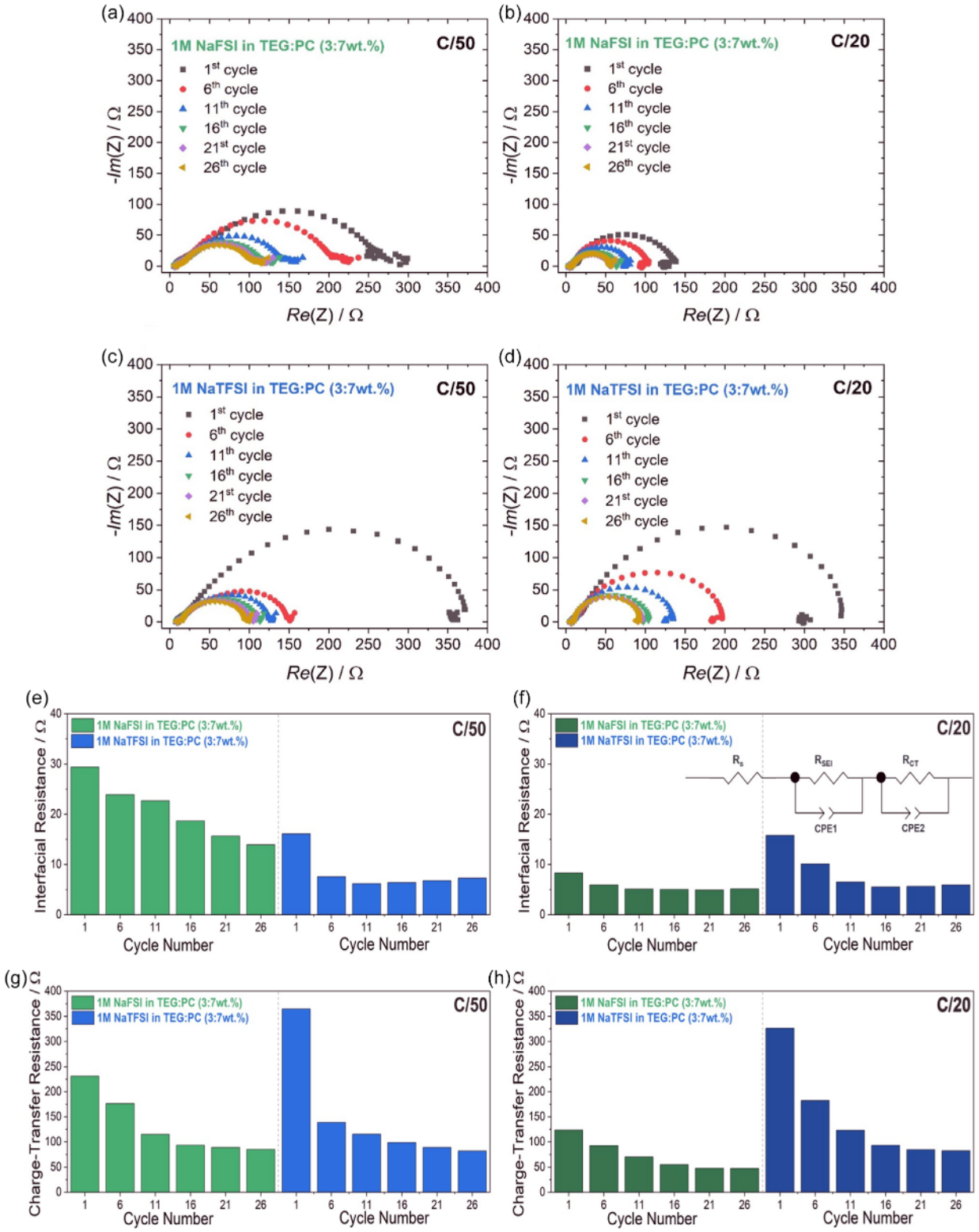

Figure 3. a–d) Nyquist plots and e–h) EIS fitting results for the interfacial resistance (R_{SEI}) and charge-transfer resistance (R_{ct}) of HC using 1 M NaFSI in TEG:PC (green), and 1 M NaTFSI in TEG:PC (blue) electrolytes after the 1st cycle at C/50 and C/20. The equivalent circuit used for fitting is shown in (f).

are aligned with the findings presented in the F 1*s* spectra, as shown in Figure S8, Supporting Information. The C 1*s* spectra for the cycled HC electrodes in both electrolytes after the 1st cycle at C/50 and C/20 show five distinctive peaks at 284.4, 285.3/285.6, 286.1/286.2, 287.4/287.6, 289.3/289.8, and 290.4/290.9 eV for NaFSI and NaTFSI in TEG:PC, which are assigned

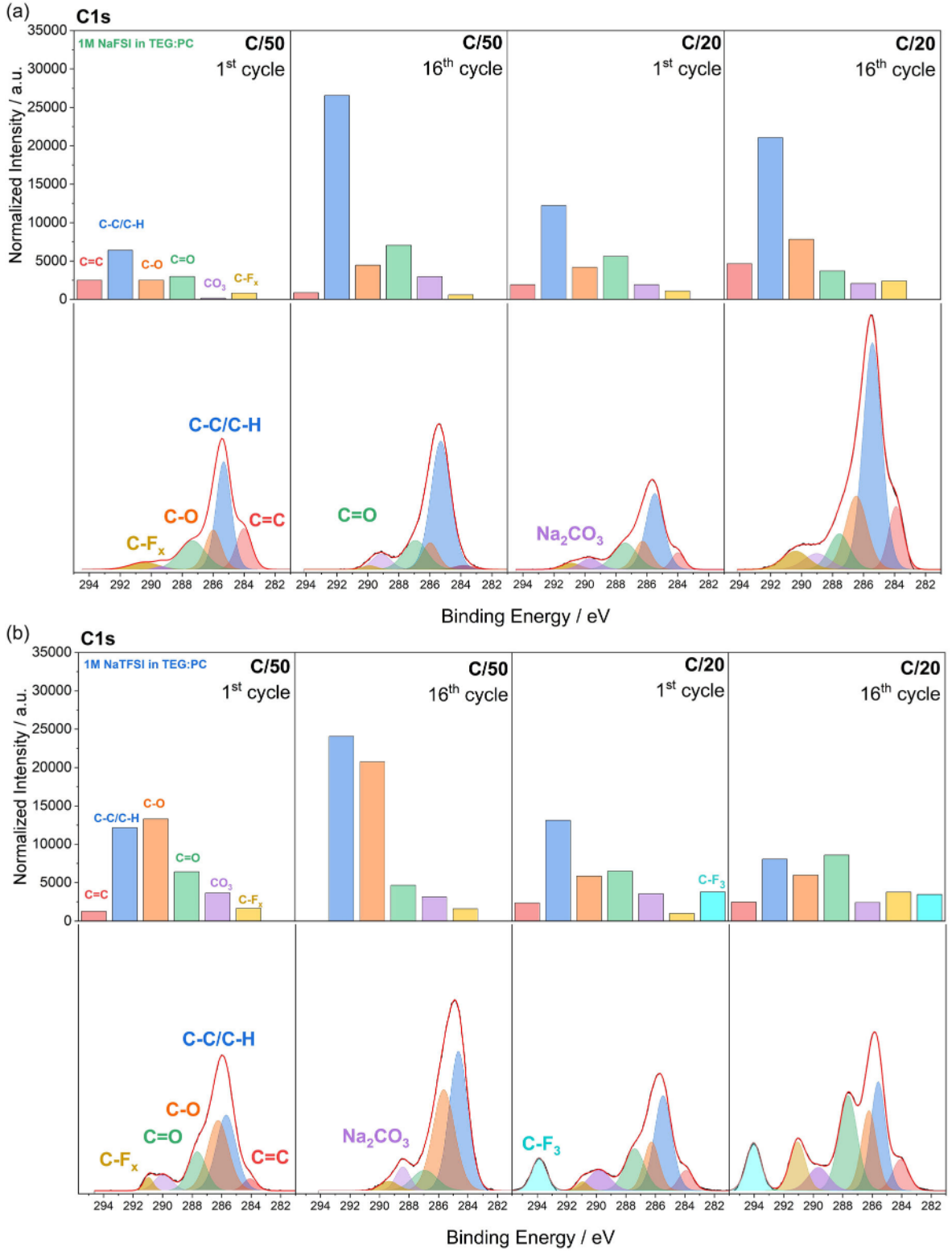

Figure 4. Fitted XPS results of cycled HC electrodes, showing the compositional distribution and the corresponding high-resolution C 1*s* spectra tested in a) 1 M NaFSI in TEG:PC, and b) 1 M NaTFSI in TEG:PC electrolytes after the 1st cycle at C/50 and C/20 and after the 16th cycle (C/2).

to the pseudo-graphitic domain of HC with sp^2-hybridized carbons (C═C), hydrocarbons (C—C/C—H), ether carbon (C—O), carbonyl carbon (C═O), sodium carbonate (Na_2CO_3) species, and compounds arising from the decomposition of the anion–solvent complex ($C\text{-}F_x$), respectively.[34,35] An additional peak at 293.8 eV for NaTFSI/TEG:PC, attributed to the $TFSI^-$ ($C\text{-}F_3$) is observed. Generally, these peaks correspond to the various carbonaceous species resulting from the PC and TEG reduction reactions, and they constitute

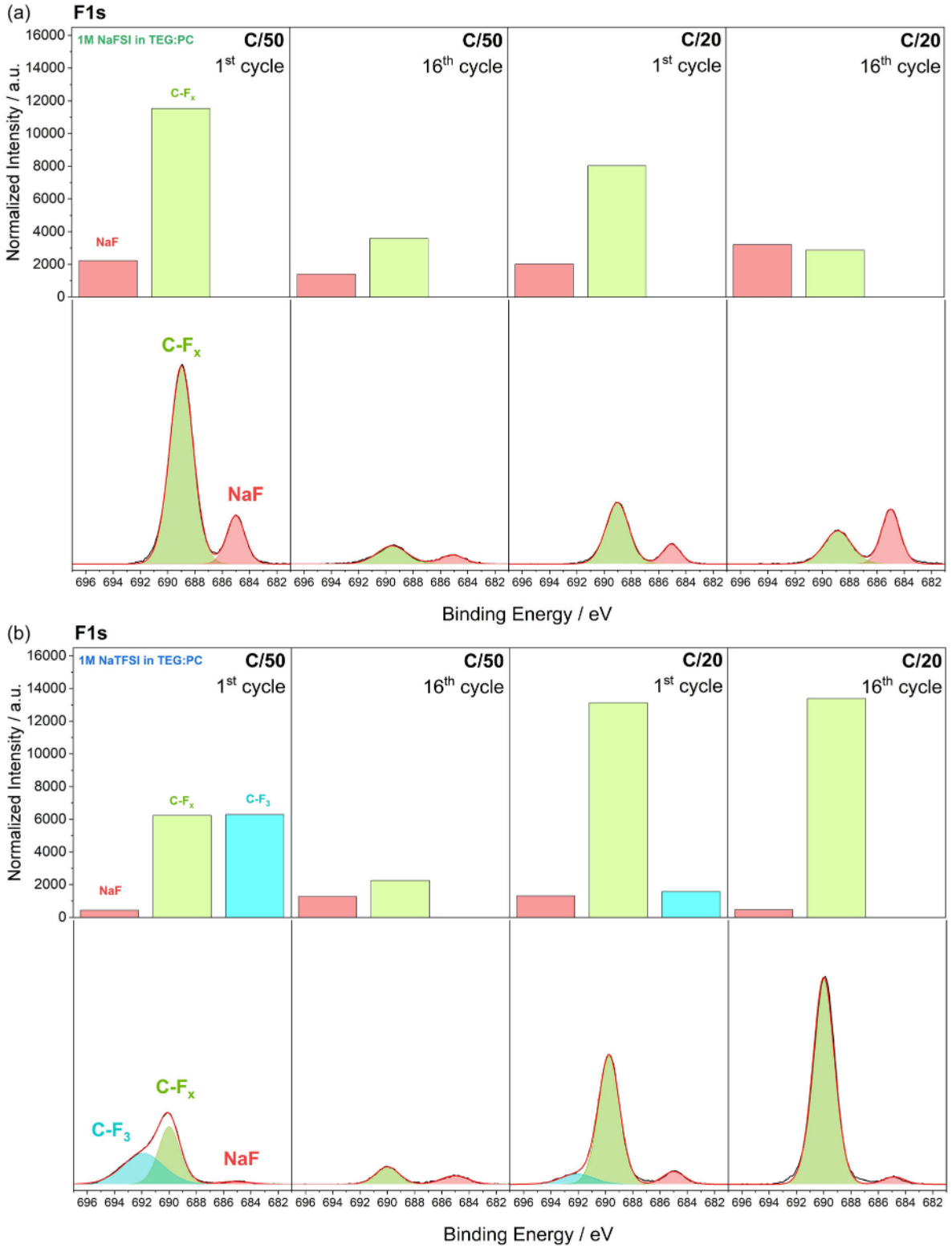

Figure 5. Fitted XPS results of cycled HC electrodes, showing the compositional distribution and the corresponding high-resolution F 1*s* spectra using a) 1 M NaFSI in TEG:PC, and b) 1 M NaTFSI in TEG:PC electrolytes after the 1st cycle at C/50 and C/20 and after the 16th cycle (C/2).

the SEI, which can be either organic, such as hydrocarbons, ethers, and sodium alkyl carbonates, or inorganic (i.e., Na_2CO_3). Furthermore, the prominence of the C=C peak in the 1st cycles in both systems and the formation rates suggest that the SEI thickness after the 1st formation cycle is below 7 nm, considering the C=C photoelectron peak and the inelastic mean free path.[36]

The F 1*s* spectra show two significant peaks at 685 and 688 eV for all systems investigated. These peaks are associated with

inorganic species, such as sodium fluoride (NaF) and other decomposition products, including reduced FSI^- and $TFSI^-$ (C-F_x) forms.[37,38] These species are formed due to the reduction of salt anions. An additional peak at 692.0 eV was observed for the HC electrode cycled in NaTFSI/TEG:PC, corresponding to $TFSI^-$ (C-F_3).[35]

For HC electrodes using NaFSI in TEG:PC, the SEI does not differ significantly in its chemical composition of detected C-species after the 1st cycle for both formation C-rates. In contrast, a distinct difference is observed in the F 1*s* spectra. After one cycle at C/50, the intensity of NaF and reduced FSI is significantly higher than at C/20, suggesting a greater decomposition of FSI^- at C/50. After 16 cycles, a reduction in the detected F-species and C-F_x signal is noted. As a result, the decomposition of FSI^- is considered complete after the 1st cycle at C/50. Subsequent cycling primarily involves the reduction of solvents, which cover the initially formed inorganic components, as evidenced by the significant increase in C—C/C—H species and a decrease in C=C bonds, indicating SEI thickening after the 16th cycle. Indeed, considering the C=C photoelectron peak, the SEI thickness can be roughly estimated to be greater than 7 nm.[36] In contrast, the thickness of the SEI after the 16th cycle, when the formation cycles are conducted at C/20, indicates that the SEI is thinner than 7 nm or highly inhomogeneous due to the presence of the C=C peak.

As a result, a bilayered SEI structure forms in NaFSI in PC:TEG, when C/50 is conducted for the formation cycle, comprising an inorganic-rich inner layer and an organic-rich outer layer. Notably, the presence of NaF near the electrode surface has been shown to enhance passivation properties by covering the HC surface, thereby mitigating SEI dissolution.[15,39] This behavior is aligned with the R_{SEI} trend, where initially higher resistance is observed due to the thicker SEI formation (more electrolyte is decomposed) and upon cycling, the SEI is accommodating, forming a well-distributed inorganic/organic bilayer, and hence reducing the R_{SEI} significantly. In contrast, at C/20, an increase in the intensity of C—C/C—H, C—O, C—F_x, and NaF signals is observed after the 16th cycle, indicating continued decomposition of both the solvent and salt upon cycling. Consequently, the ongoing electrolyte consumption leads to the formation of an SEI with a heterogeneous distribution of organic and inorganic components, which may compromise its passivating properties. This is further supported by the more pronounced C=C signal after the 16th cycle, suggesting a locally reduced coverage of the HC electrode. These factors may contribute to the improved cycling performance observed for the HC when it is initially cycled at C/50 in NaFSI in TEG:PC.

For HC paired with NaTFSI in TEG:PC, ongoing decomposition of both salt and solvents is observed after the 1st cycle. However, the extent of SEI chemical evolution is significantly lower when the cell is initially cycled at C/20. For HC electrodes subjected to a C/20 formation cycle, an increase in C—C/C—H, C—O, and C—F_x components in the C 1*s* spectrum is observed. In contrast, at C/50, the disappearance of the C=C peak suggests significant SEI thickening after 16 cycles (>7 nm, considering Tanuma´s estimations).[36] A negative shift in the binding energy of detected C-species is observed, likely resulting from a charging effect during measurement due to the increased SEI thickness. A decrease in inorganic compounds is evident from the F 1*s* spectra for C/50, indicating that the SEI composition evolves with continued cycling, leading to a notably higher accumulation of organic components at C/50.

In comparison, HC electrodes cycled in the standard $NaPF_6$-based electrolyte exhibit a chemical environment largely consistent with that of the other electrolyte systems (see Figure S9, Supporting Information). However, a higher contribution of C=O and carboxyl- (O-C=O) species, instead of organic ether-based (C—O) components, indicates an increased in inorganic content. For both formation conditions, the chemical evolution of the SEI is observed. However, the extent of the compositional changes is notably less pronounced when a current density of C/20 is applied during the 1st cycle. This observation aligns with the EIS results, suggesting a greater chemical stability of the SEI at C/20. The enhanced SEI instability and evolution over continuous cycling at C/50 is likely attributable to the higher Na_2CO_3 content after the 1st cycle. Na_2CO_3 is known to have high solubility in carbonate-based solvents.[13] Consequently, it can be inferred that the elevated concentration of Na_2CO_3 in the C/50 case contributes to the formation of a less stable and probably denser SEI due to its solubility in the EC and PC solvents. This increased solubility could result in the dissolution of the SEI upon cycling, exposing reactive sites that may lead to further electrolyte consumption. Notably, one of the key challenges in SIBs is the greater solubility of inorganic SEI components compared to their lithium-based counterparts (e.g., Li_2CO_3), a consequence of the lower Lewis acidity of Na^+.[40] Compared to $NaPF_6$/EC:PC, the Na_2CO_3 formation occurs in smaller quantities in the NaTFSI- and NaFSI-based systems, regardless of the initial C-rate. This reduced Na_2CO_3 content may mitigate SEI dissolution, even in the presence of the carbonate-based PC solvent. Density functional theory calculations indicate that the energy barrier for Na_2CO_3 formation via a two-electron reduction is 1.72 kcal mol^{-1} higher for PC than for EC, highlighting the role of EC in promoting Na_2CO_3 formation.[41] Substituting EC with TEG, thus, suppresses Na_2CO_3 formation and enhances SEI stability of HC anodes for SIBs. Although NaTFSI/TEG:PC exhibits a lower Na_2CO_3 contribution than $NaPF_6$/EC:PC, it remains higher than in NaFSI/TEG:PC. This elevated Na_2CO_3 content suggests SEI dissolution in PC, potentially contributing to differences in SEI composition and stability over cycling.

Consequently, these SEI modifications explain the improved electrochemical performance of HC with NaFSI in TEG:PC electrolyte. The differences in SEI chemistry across the systems studied can be attributed to three main factors: the substitution of EC with TEG, the use of the FSI anion instead of TFSI, and the selection of an appropriate current density during the formation cycle. First, substituting EC with TEG effectively reduces the formation of highly soluble Na_2CO_3.[13] Second, the FSI anion, which has a chemically less stable S—F bond compared to the C—F_3 bond found in $TFSI^-$, undergoes complete decomposition during the 1st cycling.[42,43] This leads to the formation of NaF, which covers the HC surface and improves passivation properties due to its low solubility in organic solvents. Lastly, the complete decomposition of the FSI anion is observed only under the C/50 formation

condition, highlighting the importance of carefully selecting an appropriate current density.

3. Conclusion

This study systematically explored the potential of substituting the commonly used $NaPF_6$ in EC:PC electrolyte with two alternative electrolytes, NaFSI and NaTFSI, in a TEG:PC mixture. The investigation focused on understanding the influence of the C-rate applied during the initial charge/discharge cycle and the choice of electrolyte formulation on the formation of the SEI on HC electrodes for SIBs. Consequently, the HC rate and cycling performance were evaluated. To correlate the differences in electrochemical performance across various electrolyte systems and to determine the impact of the initial formation cycle, a thorough analysis of the SEI properties was conducted. EIS was employed to assess the stability of the SEI during continuous cycling and to establish its relationship with Na^+ transport properties. Additionally, XPS on cycled HC electrodes was performed to characterize the surface chemistry of the SEI. In summary, this study underscores that it is not possible to make a generalized statement regarding the applicability of the C/20 current rate during the formation cycle, as various factors significantly affect this process. The research indicated that different electrolyte systems can exhibit distinct behaviors. Key elements influencing system performance include the nature of the salt and solvent, their interactions, the chemical composition of the SEI, and the distribution of SEI components (organic and inorganic). Therefore, a detailed analysis of each factor is essential.

The charge and discharge characteristics of the HC in the 1st cycle reveal that both electrolytes exhibit Na^+ storage behavior analogous to that of the standard $NaPF_6$-based electrolyte system. Notably, the use of HC in NaFSI within a TEG:PC solvent matrix yielded the highest ICE of 90% at a rate of C/50 and 92% at C/20. Furthermore, the rate and cycling performance of HC emphasize the potential of employing a 1M NaFSI in TEG:PC (3:7 wt.%) as a viable alternative to the conventional $NaPF_6$-based electrolyte. In comparison to the NaTFSI-based system, HC employing NaFSI in TEG:PC demonstrated not only a higher capacity but also stable cycling performance, with a capacity retention of 81% after 140 cycles. EIS analysis revealed a reduction in overall resistance for both electrolytes, along with stable contributions from the interfacial and charge-transfer resistances, when compared to the $NaPF_6$-based electrolyte, which exhibited a progressive increase in overall resistance during continuous cycling at an initial rate of C/50. Such degradation was not observed in the NaFSI and NaTFSI systems, highlighting their compatibility with HC in facilitating the formation of a stable SEI that reduces the barrier for Na^+ migration. XPS analysis provided further insight into the chemical composition of the SEI and its evolution throughout cycling. The increased resistance associated with the Na^+ storage process in the $NaPF_6$-based system was correlated with the formation of soluble Na_2CO_3, which may contribute to SEI dissolution in EC and PC solvents. The substitution of EC with TEG reduced the contribution of Na_2CO_3, thereby mitigating SEI dissolution and enhancing stability over cycling. Furthermore, the SEI formed on HC with the NaFSI/TEG:PC electrolyte exhibited a bilayered structure comprised of an inorganic-rich inner layer and an organic-rich outer layer, particularly under C/50 formation condition. The presence of NaF near the electrode surface was found to enhance passivation and improve interfacial stability. In contrast, the SEI formed in NaTFSI/TEG:PC displayed a greater accumulation of organic species, which may compromise its passivating properties and lead to higher resistance to Na^+ diffusion, resulting in suboptimal electrochemical performance.

These findings underscore the significant impact of electrolyte formulation on SEI formation and stability of the HC anode electrode for SIBs. Among the systems investigated, NaFSI/TEG:PC exhibited the most favorable SEI characteristics, characterized by great passivation and enhanced Na^+ transport properties, particularly following an initial formation cycle at C/50. These results open the door to alternative, safer, and more sustainable liquid electrolytes that can form an optimal SEI on the HC anodes for SIBs, thereby improving battery performance.

4. Experimental Section

Material Preparation

The herein conducted electrochemical and ex situ analyses utilize electrodes prepared from electrode sheets incorporating a commercial HC as active material. A homogenous aqueous slurry was prepared by dispersing commercial HC, sodium carboxymethylcellulose (SunroseMAC500 by Nippon Carbon Co., Ltd.), and styrene-butadiene rubber (BM-451B by Zeon) binders in a weight ratio of 94.6:1.8:3.6, respectively, in an appropriate amount of fully deionized water. The slurry was cast with a wet film thickness of 70 μm on Al foil (20 μm thickness, Korff AG) using the doctor blade technique and dried at 40 °C. The dried electrode sheet was calendered at a line pressure of 3 N mm^{-1}, and 1 m min^{-1} using a lab-calender (Sumeet). A 12 mm diameter electrodes were punched, dried in a B-585 glass vacuum oven (BÜCHI) for 60 h at 120 °C, and then weighed in a dry room (dew point <-70 °C). After an additional drying process of 20 h at 120 °C in the BÜCHI, the electrodes were transferred to an argon-filled glovebox (MBraun, H_2O, and O_2 <0.1 ppm).

Electrolyte Preparation

1 M electrolytic solutions had been prepared by dissolving $NaPF_6$ (CAS: 171 611-11-3, purity $\geq$ 99%, battery grade, Fluorochem) in a mixture of EC (CAS: 96-49-,1 purity $\geq$ 99%, Sigma-Aldrich)/PC (CAS: 108-32-7, purity $\geq$ 99%, Sigma-Aldrich; 1:1 vol.%), NaTFSI (CAS: 91 742-21-1, purity $\geq$ 99.5%, Solvionic), and NaFSI (CAS: 100 669-96-3, purity $\geq$ 99.9%, Solvionic) in TEG (CAS: 3975-14-2, Weylchem)/PC (CAS: 108-32-7, purity $\geq$ 99%, Sigma-Aldrich; 3:7 wt.%) and stored inside an argon-filled glovebox (MBraun, H_2O, and O_2 <0.1 ppm).

Electrochemical Characterization

For electrochemical analysis, three-electrode Swagelok-type cells had been used, comprising an above described HC electrode (ZSW, 70 μm wet film thickness, 12 mm diameter) with an active mass loading of 2.4–3.1 mg cm^{-2} as working electrode, and Na metal (99.8%, Across Organics) as counter and reference electrodes. Whatman GF/D glass microfiber filters (13 and 10 mm diameter), saturated with the electrolyte (160 and 80 μL), had been implemented as separators. The

cells were assembled inside an argon-filled glovebox containing less than 1 ppm of H_2O and O_2. Before testing, the assembled cells were rested for 10 h at (20 ± 1) °C for well wetting. The current densities applied were calculated based on a theoretical specific capacity of 200 mAh g^{-1} at 1C, with respect to the active mass of HC. To determine the rate capability, the half-cells were cycled within a voltage range of 2.0–0.02 V versus Na/Na^+. The 1st cycle was conducted at C/50 and C/20, while the following cycles were measured at C/10, C/5, C/3, C/2, and 1C, and then back to C/5, each for five cycles. The cycling performance was evaluated by an additional 109 cycles at C/2.

The electrochemical stability window of NaFSI in TEG:PC (3:7 wt.TR%) was determined using linear sweep voltammetry with a scan rate of 1 mV s^{-1} (VMP-3 BioLogic). A three-electrode Swagelok cell configuration was used, comprising a circular platinum disc as the working electrode, a freestanding oversized activated carbon electrode as the counter electrode, and a silver wire as the reference electrode. The glass-fiber separator (Whatman GF/D) was saturated with 160 μL of the respective electrolyte.

SEI Characterization

To analyze the evolution of the SEI over cycles, EIS was performed using a multichannel potentiostat–galvanostat (VMP3, Biologic Science Instruments) at (20 ± 1) °C within the frequency range of 5 mHz–500 kHz. The experimental configuration employed was consistent with the previously outlined three-electrode Swagelok-type setup. In this regard, the cells were cycled in a voltage range of 0.02–2.0 V versus Na/Na^+ at C/2 after an initial formation cycle of C/50 and C/20. EIS was performed after the first discharge cycle and then after following 5 cycles for 26 cycles (discharged state). The raw data were fitted using *ZView* (version 3.5i). The fit was considered reasonable when a chi-square value of less than 10^{-3} was obtained.

The surface chemical composition of the SEI was investigated using XPS. The measurements were conducted using a monochromatic Al Kα radiation ($h\nu = 1.487$ eV) X-ray source. The scans were obtained using a 200 W X-ray power source set at 12 kV, with a pass energy of 30 eV, and an energy step of 0.1 eV. Spectral fitting was performed using *CasaXPS*, applying a nonlinear Shirley-type background and a Gaussian and Lorentzian fit function (GL(30)). The calibration of the binding energy was performed using the sodium fluoride (NaF) peak at 685.0 eV.[31] Before conducting the XPS measurements, the cycled cells were disassembled inside the glovebox. The HC electrodes were then rinsed with DMC. After drying inside the glovebox's prechamber under vacuum for 30 min, and transferred to the XPS chamber using an air-tight transfer box to prevent any contact with the atmosphere, which could alter the SEI composition.

Acknowledgements

The authors acknowledge financial support from the BMFTR Transition Transfer project (FZK 03XP0533). M.Z. also thanks the Helmholtz Association for financial support. L.P. and A.P. thank Paul Drews (ZSW) for the preparation of HC electrode sheets.

Conflict of Interest

The authors declare no conflict of interest.

Data Availability Statement

The data that support the findings of this study are available on request from the corresponding author. The data are not publicly available due to privacy or ethical restrictions.

Keywords: 1,1,2,2-tetraethoxyglyoxal · carbonate-based electrolytes · hard carbons · solid electrolyte interphases · sodium-ion batteries

[1] T. Chen, Y. Jin, H. Lv, A. Yang, M. Liu, B. Chen, Y. Xie, Q. Chen, *Trans. Tianjin Univ.* **2020**, *26*, 208.
[2] S. Zhao, Z. Guo, K. Yan, S. Wan, F. He, B. Sun, G. Wang, *Energy Storage Mater.* **2021**, *34*, 716.
[3] K. Sada, J. Darga, A. Manthiram, *Adv. Energy Mater.* **2023**, *13*, 2302321.
[4] M. Liu, Y. Wang, F. Wu, Y. Bai, Y. Li, Y. Gong, X. Feng, Z. Wang, C. Wu, *Adv. Funct. Mater.* **2022**, *32*, 2203117.
[5] E. Quartarone, T. Eisenmann, M. Kuenzel, C. Tealdi, A. G. Marrani, S. Brutti, D. Callegari, S. Passerini, *J Electrochem. Soc.* **2020**, *167*, 080509.
[6] Group1.ai | Critical-Mineral-Free Potassium-ion Batteries. https://group1.ai/, (accessed: April 2025).
[7] What Is Natron - Our History | Natron Energy. https://natron.energy/company/growth-trajectory, (accessed: May 2024).
[8] CATL Unveils Its Latest Breakthrough Technology by Releasing Its First Generation of Sodium-ion Batteries. https://www.catl.com/en/news/665.html, (accessed: April 2025).
[9] HiNa Battery Technology Co., Ltd. https://www.hinabattery.com/en/, (accessed: April 2025).
[10] C. Bommier, X. Ji, *Small* **2018**, *14*, 1703576.
[11] Y. Sun, P. Shi, H. Xiang, X. Liang, Y. Yu, *Small* **2019**, *15*, 1805479.
[12] Achievements - Research & Development - HiNa Battery Technology Co., Ltd. https://www.hinabattery.com/en/index.php?catid=15, (accessed: April 2025).
[13] L. A. Ma, A. J. Naylor, L. Nyholm, R. Younesi, *Angew. Chem. Int. Ed.* **2021**, *133*, 4905.
[14] M. Ma, H. Cai, C. Xu, R. Huang, S. Wang, H. Pan, Y.-S. Hu, *Adv. Funct. Mater.* **2021**, *31*, 2100278.
[15] Y. Li, F. Wu, Y. Li, M. Liu, X. Feng, Y. Bai, C. Wu, *Chem. Soc. Rev.* **2022**, *51*, 4484.
[16] K. Li, J. Zhang, D. Lin, D.-W. Wang, B. Li, W. Lv, S. Sun, Y.-B. He, F. Kang, Q.-H. Yang, L. Zhou, T.-Y. Zhang, *Nat. Commun.* **2019**, *10*, 725.
[17] K. Westman, R. Dugas, P. Jankwski, W. Wieczorek, G. Gachot, M. Morcrette, E. Irisarri, A. Ponrouch, M. R. Palacin, J. M. Tarascon, P. Johansson, *ACS Appl. Energy Mater.* **2018**, *1*, 2671.
[18] L. M. Kha, V. D. Thanh, N. Van Hoang, L. Van Thang, L. M. L. Phung, *Vietnam J. Chem.* **2020**, *58*, 643.
[19] L. H. Heß, A. Balducci, *ChemSusChem* **2018**, *11*, 1919.
[20] L. Gehrlein, C. Leibing, K. Pfeifer, F. Jeschull, A. Balducci, J. Maibach, *Electrochim. Acta* **2022**, *424*, 140642.
[21] S. Liu, L. C. Meyer, L. Medenbach, A. Balducci, *Energy Storage Mater.* **2022**, *47*, 534.
[22] C. Leibing, A. Balducci, *J. Electrochem. Soc.* **2021**, *168*, 090533.
[23] C. Leibing, D. Leistenschneider, C. Neumann, M. Oschatz, A. Turchanin, A. Balducci, *ChemSusChem* **2023**, *16*, e202300161.
[24] L. Köps, C. Leibing, L. H. Hess, A. Balducci, *J. Electrochem. Soc.* **2021**, *168*, 010513.
[25] X. Han, L. Lu, Y. Zheng, X. Feng, Z. Li, J. Li, M. Ouyang, *eTransportation* **2019**, *1*, 100005.
[26] M. Usman Tahir, A. Sangwongwanich, D.-I. Stroe, F. Blaabjerg, *J. Energy Chem.* **2023**, *84*, 228.
[27] S. Hess, M. Wohlfahrt-Mehrens, M. Wachtler, *J. Electrochem. Soc.* **2015**, *162*, A3084.
[28] Y. Morikawa, S. Nishimura, R. Hashimoto, M. Ohnuma, A. Yamada, *Adv. Energy Mater.* **2020**, *10*, 1903176.
[29] S. Tan, H. Yang, Z. Zhang, X. Xu, Y. Xu, J. Zhou, X. Zhou, Z. Pan, X. Rao, Y. Gu, Z. Wang, Y. Wu, X. Liu, Y. Zhang, *Molecules* **2023**, *28*, 3134.
[30] X. Dou, I. Hasa, M. Hekmatfar, T. Diemant, R. J. Behm, D. Buchholz, S. Passerini, *ChemSusChem* **2017**, *10*, 2668.
[31] H. Moon, M. Zarrabeitia, E. Frank, O. Böse, M. Enterría, D. Saurel, I. Hasa, S. Passerini, *Batteries Supercaps* **2021**, *4*, 960.

[32] H. Moon, A. Innocenti, H. Liu, H. Zhang, M. Weil, M. Zarrabeitia, S. Passerini, *ChemSusChem* **2023**, *16*, e202201713.
[33] M. Van Haeverbeke, M. Stock, B. De Baets, *IEEE Access* **2022**, *10*, 51363.
[34] M. C. Biesinger, *Appl. Surf. Sci.* **2022**, *597*, 153681.
[35] G. Beamson, D. Briggs, *J. Chem. Educ.* **1993**, *70*, A25.
[36] S. Tanuma, C. J. Powell, D. R. Penn, *Surf. Interfaces Anal.* **2011**, *43*, 689.
[37] X-ray Photoelectron Spectroscopy (XPS) Reference Pages: Fluorine. https://www.xpsfitting.com/2017/05/fluorine.html. (accessed: April 2025).
[38] G. G. Eshetu, T. Diemant, M. Hekmatfar, S. Grugeon, R. J. Behm, S. Laurelle, M. Armand, S. Passerini, *Nano Energy* **2019**, *55*, 327.
[39] Z. Tang, H. Wang, P.-F. Wu, S.-Y. Zhou, Y.-C. Huang, R. Zhang, D. Sun, Y.-G. Tang, H.-Y. Wang, *Angew. Chem. Int. Ed.* **2022**, *61*, e202200475.
[40] R. Mogensen, D. Brandell, R. Younesi, *ACS Energy Lett.* **2016**, *1*, 1173.
[41] Q. Liu, D. Mu, B. Wu, L. Wang, L. Gai, F. Wu, *ChemSusChem* **2017**, *10*, 786.
[42] M. Phuong Do, N. Bucher, A. Nagasubramanian, I. Markovits, T. Bingbing, P. J. Fischer, K. Ping Loh, F. E. Kühn, M. Srinivasan, *ACS Appl. Mater. Interfaces* **2019**, *11*, 23972.
[43] K. Takada, Y. Yamada, E. Watanabe, J. Wang, K. Sodeyama, Y. Tateyana, K. Hirata, T. Kawase, A. Yamada, *ACS Appl. Mater. Interfaces* **2017**, *9*, 33802.

Manuscript received: April 17, 2025
Revised manuscript received: June 20, 2025
Version of record online: